




# Catalytic hydrolysis of sodium borohydride for hydrogen generation using g-C<sub>3</sub>N<sub>4</sub>/Co–W–B/Ni foam composite catalyst

Haiyue Cong<sup>1</sup>, Jian Ren<sup>1</sup>, Di Zhang<sup>1</sup>, Fengyan Xu<sup>1</sup>, Xue Wang<sup>1</sup>, Yan Wang<sup>1,2,\*</sup> , Ke Zhang<sup>1</sup>, Zhongqiu Cao<sup>1</sup>, Guode Li<sup>3</sup>, and Shiwei Wu<sup>4</sup>

<sup>1</sup>Institute of Catalysis for Energy and Environment, College of Chemistry and Chemical Engineering, Shenyang Normal University, Shenyang 110034, People's Republic of China

<sup>2</sup>Key Laboratory of Advanced Energy Materials Chemistry (Ministry of Education), Nankai University, Tianjin 300071, People's Republic of China

<sup>3</sup>Office of Academic Research, Shenyang Normal University, Shenyang 110034, People's Republic of China

<sup>4</sup>Experimental Center, Shenyang Normal University, Shenyang 110034, People's Republic of China

Received: 26 August 2022

Accepted: 7 December 2022

Published online:

1 January 2023

© The Author(s), under exclusive licence to Springer Science+Business Media, LLC, part of Springer Nature 2022

## ABSTRACT

In this study, electroless plating method was adopted for the first time to prepare double-loaded g-C<sub>3</sub>N<sub>4</sub>/Co–W–B/NF (NF = Ni foam) catalysts. Different g-C<sub>3</sub>N<sub>4</sub>/Co–W–B/NF catalysts were obtained by changing the molar ratio of initial Co<sup>2+</sup> and WO<sub>4</sub><sup>2-</sup> ( $n_{\text{Co}^{2+}} : n_{\text{WO}_4^{2-}}$ ) in the catalyst plating solution, and their catalytic effects were tested for catalyzing hydrolysis of NaBH<sub>4</sub> solution to release hydrogen (H<sub>2</sub>). Among them, when  $n_{\text{Co}^{2+}} : n_{\text{WO}_4^{2-}}$  value was 5:5, g-C<sub>3</sub>N<sub>4</sub>/Co–W–B/NF exhibited the best catalytic activity on the hydrolysis of NaBH<sub>4</sub> solution. Its released H<sub>2</sub> rate was 7328 mL·min<sup>-1</sup> g<sup>-1</sup> under visible light irradiation, which outperformed 6191 mL·min<sup>-1</sup> g<sup>-1</sup> of g-C<sub>3</sub>N<sub>4</sub>/Co–B/NF catalyst. The activation energy reduced from 45.6 kJ mol<sup>-1</sup> of g-C<sub>3</sub>N<sub>4</sub>/Co–B/NF to 31.5 kJ mol<sup>-1</sup> of g-C<sub>3</sub>N<sub>4</sub>/Co–W–B/NF under visible light irradiation. The result showed that adding an appropriate amount of W played a significant role in promoting the catalytic performance in NaBH<sub>4</sub> hydrolysis. Moreover, under visible light irradiation, a possible mechanism was proposed on g-C<sub>3</sub>N<sub>4</sub>/Co–W–B/NF catalyst toward the H<sub>2</sub> generation from NaBH<sub>4</sub> hydrolysis.

Handling Editor: Pedro Camargo.

Address correspondence to E-mail: wangyan11287@mail.nankai.edu.cn

<https://doi.org/10.1007/s10853-022-08073-z>

## Introduction

At present, the reserves of fossil fuels (e.g., coal, oil, natural gas) are becoming depleted, and at the same time, the massive use of fossil fuels has also caused serious damage to the environment. It is urgent to find a clean and efficient energy source with large reserves. Hydrogen energy is known as the most promising renewable energy in the future because of its high thermal value, pollution-free combustion products, and renewable characteristics [1–4]. But there is no large-scale input production and use due to its difficulties in production, storage, transportation, and so on. In order to solve related H<sub>2</sub> problems, chemical hydrogen storage materials with high hydrogen content have caused the wide concern of scientific researchers [5, 6]. In recent years, high-capacity hydrogen storage materials have been developed, including sodium borohydride (NaBH<sub>4</sub>) [7], lithium borohydride (LiBH<sub>4</sub>) [8], sodium aluminum hydride (NaAlH<sub>4</sub>) [9], and so on. Among them, NaBH<sub>4</sub> has gained more attention due to its high hydrogen storage capacity (10.8 wt%), cheap cost, and good stability in alkaline solutions [10]. Furthermore, the stored hydrogen can be released by the means of the catalytic hydrolysis of alkaline NaBH<sub>4</sub> solution at room temperature, whose hydrolysis equation is as follows [11]:



It should be pointed out that the by-product is nontoxic and harmless recyclable regeneration [12]. However, the rate of hydrogen production from NaBH<sub>4</sub> hydrolysis is slow for this reaction, which necessitates the selection of an efficient catalyst to improve the rate. So far, researchers from around the world have conducted extensive researches on the performance and stability of various types of catalysts for catalyzing NaBH<sub>4</sub> hydrolysis for hydrogen production. Common catalysts can be divided into two categories, including noble metal-based [13] and non-noble metal-based catalysts [14, 15]. Although noble metal catalysts exhibit excellent catalysis, their wide applications are limited by their expensive price and limited metal reserves. Comparatively, non-noble metal catalysts, represented by cobalt based and nickel based catalysts, are gaining much favor due to their low price and mild reaction temperature. Among them, cobalt based catalysts are more

attractive because of their high redox chemical activity and wide range of oxidation states [16].

However, the catalytic activity of non-noble metal-based catalysts still has a certain gap compared with noble metals in their catalytic performance, and there is still much room for practical catalytic effect as well as stability. People utilize the synergy between non-noble metals and special electron transfer path to improve the performance of catalysts. Sahiner et al. [17] prepared the Co–Ni bimetallic catalyst by dual use of hydrogel. The catalysts showed high yield during to generate hydrogen in the hydrolysis of NaBH<sub>4</sub>. Gradually, binary, ternary, and other multiple composite catalysts are prepared and applied to catalyze the hydrolysis of NaBH<sub>4</sub> for hydrogen production. The multiple composite type of cobalt based catalysts exhibited much better catalytic performance relative to the single component cobalt based catalysts [18]. Based on the above consideration, in order to further improve the ability of the catalytic NaBH<sub>4</sub> hydrolysis for hydrogen production, graphite-like carbon nitride (g-C<sub>3</sub>N<sub>4</sub>) was added during preparing the catalyst in this experiment. g-C<sub>3</sub>N<sub>4</sub> has photocatalytic properties, and its photocatalytic mechanism is mainly determined by its unique electron rich structure, which can realize the half-reaction of continuous and efficient catalytic hydrogen production with the assistance of sacrificial agents and cocatalysts [19]. Meanwhile, the g-C<sub>3</sub>N<sub>4</sub> surface contains functional groups such as amino groups, which can not only more effectively stabilize the metal nanoparticles but also benefit the dispersion of g-C<sub>3</sub>N<sub>4</sub> in aqueous solution and other polar solvents [20]. Based on this special property, catalysts with certain photocatalytic characteristics can be fabricated, which can effectively improve the catalytic effect of catalysts under the irradiation of visible light. Guo et al. [21] prepared a series of C<sub>3</sub>N<sub>4</sub>-immobilized bimetallic AuM (M = Co, Ni) as catalysts for hydrolytic dehydrogenation of ammonia borane (NH<sub>3</sub>BH<sub>3</sub>). Liu et al. [22] reported g-C<sub>3</sub>N<sub>4</sub>@Ni<sub>3</sub>C nanosheets for the hydrogen generation via NaBH<sub>4</sub> hydrolysis. However, the photocatalytic properties of the hydrolysis of NH<sub>3</sub>BH<sub>3</sub> or NaBH<sub>4</sub> have not been discussed. In 2018, Navlani-García et al. [23] investigated the visible-light-enhanced catalytic activity of Ru nanoparticles over carbon modified g-C<sub>3</sub>N<sub>4</sub> for the hydrolysis of NH<sub>3</sub>BH<sub>3</sub>, which supplied a new strategy for the hydrogen generation.

It is well known that the development of catalysts depends on the type of process. Catalysts can be prepared in the form of coatings or powders. Generally, powder catalysts can be obtained by liquid phase reduction method, which squints toward forming aggregates and requires very complicated separation and washing procedures to achieve recyclability; nevertheless, powder type catalysts do not have the ability to produce hydrogen as needed [24]. Therefore, the thin-film catalysts are considered as the desired type, which can be synthesized by electro-deposition or electroless plating method. The catalysts can avoid the above problems. Especially, it is convenient to recover and separate, and the rate of catalytic  $\text{NaBH}_4$  hydrolysis is controllable. Among numerous substrate materials to prepare the thin-film catalyst, the Ni foam is extensively employed because of its unique 3D structure, which can effectively restrain the particle agglomeration when compared with the traditional powdery catalyst.

In this study, we prepare double-loaded  $\text{g-C}_3\text{N}_4/\text{Co-W-B/NF}$  (NF = Ni foam) catalyst in the form of coating for the first time using electroless plating method. The catalytic property for the hydrolysis of  $\text{NaBH}_4$  solution was observed under visible light irradiation. Compared with single metal  $\text{g-C}_3\text{N}_4/\text{Co-B/NF}$  catalyst, bimetallic  $\text{g-C}_3\text{N}_4/\text{Co-W-B/NF}$  shows good catalytic with high released  $\text{H}_2$  rate and lower activation energy. In addition, the catalytic mechanism of  $\text{NaBH}_4$  hydrolysis is forecasted in the presence of  $\text{g-C}_3\text{N}_4/\text{Co-W-B/NF}$  catalyst.

## Experimental

### Chemical reagents

Most of the chemical reagents were purchased from Sinopharm Chemical Reagent Co., Ltd., except for  $\text{NaBH}_4$  (96% purity, Sigma Aldrich), and employed without further purification. The detailed information is as follows:  $\text{NaOH}$  (AR,  $\text{NaOH}$ ),  $\text{SnCl}_2$  (98% purity),  $\text{PbCl}_2$  (59% purity),  $\text{CoCl}_2 \cdot 6\text{H}_2\text{O}$  (99.7% purity),  $\text{Na}_2\text{WO}_4 \cdot 2\text{H}_2\text{O}$  (99% purity) and  $\text{C}_2\text{H}_5\text{NO}_2$  (96% purity). Carbon nitride ( $\text{g-C}_3\text{N}_4$ , 99% purity) was derived from Dongguan Bonte Surface Treatment Material Co., LTD. Figure 1S shows the SEM image of the purchased  $\text{g-C}_3\text{N}_4$ . It can be seen that  $\text{g-C}_3\text{N}_4$  exhibited a two-dimensional structure with a rugged surface.

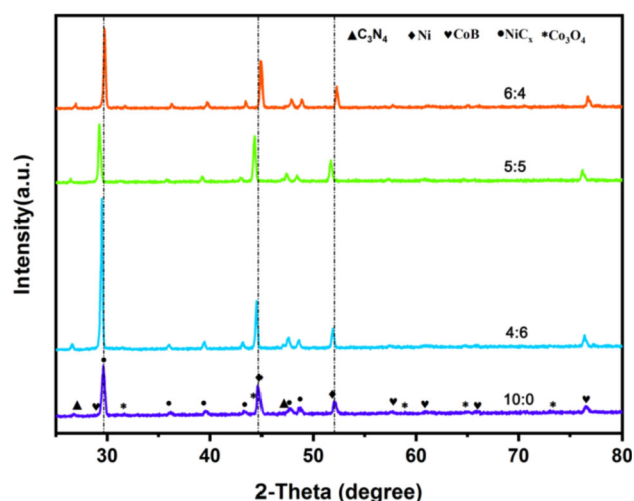


**Figure 1** XRD patterns of  $\text{g-C}_3\text{N}_4/\text{Co-W-B/NF}$  samples prepared under different  $n_{\text{Co}^{2+}} : n_{\text{WO}_4^{2-}}$  values.

### Pretreatment of Ni foam

Ni foam with a surface area of  $4 \times 4 \text{ cm}^2$  was selected as the substrate for  $\text{g-C}_3\text{N}_4/\text{Co-B}$  and  $\text{g-C}_3\text{N}_4/\text{Co-W-B}$  catalysts. The erosion fluid was composed of 10 wt. %  $\text{HCl}$  aqueous solution. The sensitization solution and activating solution consisted of  $1 \text{ g} \cdot \text{L}^{-1}$   $\text{SnCl}_2 + 1 \text{ mL} \cdot \text{L}^{-1}$   $\text{HCl}$  and  $0.1 \text{ g} \cdot \text{L}^{-1}$   $\text{PdCl}_2$  and  $1 \text{ mL} \cdot \text{L}^{-1}$   $\text{HCl}$ , respectively. Prior to the preparation of catalysts, the Ni foam substrate needs to be pretreated. 2 g of sodium hydroxide mixed with 50 ml of distilled water and heated to  $60 \text{ }^\circ\text{C}$ , and then, the Ni foam was put into the hot solution and fully soaked for 3 min. After that, the Ni foam was placed into the erosion fluid for 3 min. After removal, the Ni foam was successively washed with distilled water and absolute ethyl alcohol three times and dried in a vacuum drying oven. The dried Ni foam was put into the sensitization solution and immersed thoroughly for 3 min for sensitization, while the activation solution was immersed thoroughly for 2 min for activation. Finally, they were washed again and put in vacuum drying oven to dry and then weighed, and the mass was noted as  $m_1$ .

### Configuration of bath

$0.1 \text{ g} \cdot \text{g-C}_3\text{N}_4$  was put into 80 mL distilled water and ultrasonically dispersed for 30 min to form dispersion.  $0.06 \text{ mol L}^{-1}$   $\text{NH}_2\text{CH}_2\text{COOH}$ ,  $0.05 \text{ mol L}^{-1}$   $\text{CoCl}_2 \cdot 6\text{H}_2\text{O}$ ,  $0.05 \text{ mol L}^{-1}$   $\text{Na}_2\text{WO}_4 \cdot 2\text{H}_2\text{O}$  were added into the dispersion and stirred until dissolved.

0.4 mol L<sup>-1</sup> NaBH<sub>4</sub> was used as the reducing agent. The total molar content of Co<sup>2+</sup> and WO<sub>4</sub><sup>2-</sup> in the bath was kept to be 0.1 mol. The pH value in the solution was regulated to 11.0 with aqueous sodium hydroxide.

### Preparation of g-C<sub>3</sub>N<sub>4</sub>/Co-W-B/NF and g-C<sub>3</sub>N<sub>4</sub>/Co-B/NF catalysts

At 298 K, the pretreated Ni foam substrate was placed into the configured bath for 5 min. The deposited g-C<sub>3</sub>N<sub>4</sub>/Co-W-B/NF was removed from the solution, cleaned and then put into vacuum desiccator to dry. Finally, the dried the g-C<sub>3</sub>N<sub>4</sub>/Co-W-B/NF sample was synthesized. The mass of the weighed g-C<sub>3</sub>N<sub>4</sub>/Co-W-B/NF is denoted as m<sub>2</sub>. The mass of g-C<sub>3</sub>N<sub>4</sub>/Co-W-B catalysts can be calculated and expressed as the equation of m<sub>catalyst</sub> = m<sub>2</sub> - m<sub>1</sub>. To investigate the effect of the molar ratios of Co<sup>2+</sup> and WO<sub>4</sub><sup>2-</sup> (n<sub>Co<sup>2+</sup></sub>: n<sub>WO<sub>4</sub><sup>2-</sup></sub>) on the catalytic property of the prepared g-C<sub>3</sub>N<sub>4</sub>/Co-W-B catalyst samples, the values of n<sub>Co<sup>2+</sup></sub>: n<sub>WO<sub>4</sub><sup>2-</sup></sub> were modified to 10:0, 4:6, 5:5, 6:4. When the molar ratio of Co<sup>2+</sup> and WO<sub>4</sub><sup>2-</sup> is 10:0, the obtained sample can be labeled as g-C<sub>3</sub>N<sub>4</sub>/Co-B/NF.

### Catalyst performance tests

G-C<sub>3</sub>N<sub>4</sub>/Co-B/NF and different g-C<sub>3</sub>N<sub>4</sub>/Co-W-B/NF samples prepared in this work were tested for H<sub>2</sub> production by catalytic NaBH<sub>4</sub> hydrolysis, and the volume of released H<sub>2</sub> was recorded using a water displacement method [25]. The detailed steps were as follows: 10 mL sodium borohydride basic aqueous solution (1 wt. % NaOH + 5 wt. % NaBH<sub>4</sub>) was placed into a three-necked round-bottom flask with temperature control device to 298 K. Then, a certain amount of g-C<sub>3</sub>N<sub>4</sub>/Co-B/NF catalyst was completely dipped into the aforementioned solution without stirring. The catalyst weight was calculated on the basis of the mass of g-C<sub>3</sub>N<sub>4</sub>/Co-B, excluding the weight of Ni foam. The volume of the evolved H<sub>2</sub> was recorded every fixed time. After the hydrolysis reaction is completed, the catalyst was extracted, washed, and dried. To examine whether the g-C<sub>3</sub>N<sub>4</sub> photocatalytic performance could play a role in the prepared catalysts, the same catalysts were therefore tested for H<sub>2</sub> evolution under darkness and visible light irradiation. The darkness experiment was operated in darkroom. For the latter, a xenon lamp

was installed above the flask to perform the reaction under visible-light irradiation. The reaction was accomplished under an irradiation of 350 W xenon lamp with 420 nm cutoff filter (ZYP350W). The reaction solution was 15 cm from the exit of light. H<sub>2</sub> evolution from NaBH<sub>4</sub> hydrolysis was catalyzed at different hydrolysis temperatures using the optimized catalyst to ascertain the activation energy of the reaction.

### Catalyst characterization

X-ray diffractometer (XRD) patterns of different g-C<sub>3</sub>N<sub>4</sub>/Co-W-B/NF catalysts were gained with Rigaku-Dmax 2500 at Cu Kα radiation (λ = 1.54178 Å) to subject to material phase analysis. The morphology and structure of catalysts were researched by scanning electron microscopy (SEM) using a Hitachi s-4800. The elemental chemical states of Co, W, B, C, and N in g-C<sub>3</sub>N<sub>4</sub>/Co-W-B/NF catalysts were recorded by X-ray photoelectron spectroscopy (XPS) on VG Multilab 2000.

## Results and discussion

### Catalyst characterization

The XRD patterns of g-C<sub>3</sub>N<sub>4</sub>/Co-W-B/NF samples prepared under different n<sub>Co<sup>2+</sup></sub>: n<sub>WO<sub>4</sub><sup>2-</sup></sub> values are shown in Fig. 1. For various g-C<sub>3</sub>N<sub>4</sub>/Co-W-B/NF samples, there are similar phase compositions. It can be clearly observed the diffraction peaks of NiC<sub>x</sub> (JCPDS NO. 45–0979) and metal Ni (JCPDS NO. 3–1051) as the constituents of Ni foam substrate. The diffraction peaks at 2θ = 26.5° and 46.9° can be attributed to g-C<sub>3</sub>N<sub>4</sub> phase, indicating that g-C<sub>3</sub>N<sub>4</sub> has been successfully introduced the catalyst system. In addition, a series of diffraction peaks with weak intensity can be assigned to the CoB phase (JCPDS NO. 45–0979) [26] and Co<sub>3</sub>O<sub>4</sub> phase (JCPDS NO. 45–0979). The appearance of Co<sub>3</sub>O<sub>4</sub> may due to the oxidation of metal Co during the synthesis and storage process of catalysts. Compared with the XRD pattern of g-C<sub>3</sub>N<sub>4</sub>/Co-B/NF, the peaks of g-C<sub>3</sub>N<sub>4</sub>/Co-W-B/NF (n<sub>Co<sup>2+</sup></sub>: n<sub>WO<sub>4</sub><sup>2-</sup></sub> = 4 : 6) and g-C<sub>3</sub>N<sub>4</sub>/Co-W-B/NF (n<sub>Co<sup>2+</sup></sub>: n<sub>WO<sub>4</sub><sup>2-</sup></sub> = 5 : 5) significantly shift to the small angle, illustrating that the W atom has been doped into the g-C<sub>3</sub>N<sub>4</sub>/Co-B/NF, especially for g-C<sub>3</sub>N<sub>4</sub>/Co-W-B/NF (n<sub>Co<sup>2+</sup></sub>: n<sub>WO<sub>4</sub><sup>2-</sup></sub> = 5 : 5). That is to say, when

the initial molar ratio of  $\text{Co}^{2+}$  and  $\text{WO}_4^{2-}$  is 5:5, the doping amount of W atom is relatively high. Moreover, the peak intensities of  $\text{g-C}_3\text{N}_4/\text{Co-W-B/NF}$  ( $n_{\text{Co}^{2+}}:n_{\text{WO}_4^{2-}} = 5:5$ ) are weaker, signifying that the particle size is smaller when compared to  $\text{g-C}_3\text{N}_4/\text{Co-W-B/NF}$  ( $n_{\text{Co}^{2+}}:n_{\text{WO}_4^{2-}} = 4:6$ ) and  $\text{g-C}_3\text{N}_4/\text{Co-W-B/NF}$  ( $n_{\text{Co}^{2+}}:n_{\text{WO}_4^{2-}} = 6:4$ ). It can supply larger specific surface area, creating more active sites on the surface, which benefits the improvement in catalytic performance.

The surface morphologies of the prepared  $\text{g-C}_3\text{N}_4/\text{Co-W-B/NF}$  samples under different  $n_{\text{Co}^{2+}}:n_{\text{WO}_4^{2-}}$  values are observed by scanning electron microscope (SEM). Figure 2a–c, d–f, g–i and j–l shows the SEM images and the corresponding size distributions of various  $\text{g-C}_3\text{N}_4/\text{Co-W-B/NF}$  samples with different magnification, respectively. As shown in Fig. 2, these samples manifest the kinked banded structure with lots of nanoparticles. As the  $n_{\text{Co}^{2+}}:n_{\text{WO}_4^{2-}}$  value gradually increases from 4:6 to 6:4, the number of catalyst particles is also increasing and the particle size is gradually reduced on the surface of Ni foam from 145 to 82 nm (Fig. 2a–i). However, further increasing  $n_{\text{Co}^{2+}}:n_{\text{WO}_4^{2-}}$  to 10:0, the particle size is expanded to 202 nm. As depicted in Fig. 2d and e, the banded structure of  $\text{g-C}_3\text{N}_4/\text{Co-W-B/NF}$  is extremely special when  $n_{\text{Co}^{2+}}:n_{\text{WO}_4^{2-}}$  reaches 5:5. Firstly, partial hollow structure stacked by many particles can be clearly seen on the surface, and secondly, the particle size is smaller than that of  $\text{g-C}_3\text{N}_4/\text{Co-W-B/NF}$  ( $n_{\text{Co}^{2+}}:n_{\text{WO}_4^{2-}} = 4:6$ ) and  $\text{g-C}_3\text{N}_4/\text{Co-W-B/NF}$  ( $n_{\text{Co}^{2+}}:n_{\text{WO}_4^{2-}} = 10:0$ ), and the bumpy trend is more severe than  $\text{g-C}_3\text{N}_4/\text{Co-W-B/NF}$  ( $n_{\text{Co}^{2+}}:n_{\text{WO}_4^{2-}} = 6:4$ ). Consequently, it can be inferred that  $\text{g-C}_3\text{N}_4/\text{Co-W-B/NF}$  ( $n_{\text{Co}^{2+}}:n_{\text{WO}_4^{2-}} = 5:5$ ) can offer the maximum specific surface area on the catalyst surface. As reported by Eom et al. [27], it is more favorable to accelerate the gas transmission and achieve the improvement in catalytic activity.

To further investigate and explore the basic chemical states of the individual elements in the as-synthesized  $\text{g-C}_3\text{N}_4/\text{Co-W-B/NF}$  ( $n_{\text{Co}^{2+}}:n_{\text{WO}_4^{2-}} = 5:5$ ) sample, XPS spectroscopic studies are performed in Fig. 3. The survey of XPS spectrum in Fig. 3a shows the presence of Co, W, B, C, and N elements. Figure 3b displays the fitting XPS spectrum for the partial peaks of Co 2p; it can be seen

that there are two typical characteristic peaks located at 780.6 eV and 782.2 eV for the Co 2P<sub>3/2</sub> level, assigning to  $\text{Co}^{3+}$  and  $\text{Co}^{2+}$  [28, 29], respectively. Moreover, the difference of bonding energy ( $\Delta E$ ) between Co 2P<sub>3/2</sub> and Co 2P<sub>1/2</sub> is measured to be 15.2 eV, which also demonstrates that Co species exists in the form of  $\text{Co}^{3+}$  and  $\text{Co}^{2+}$  [30]. The XPS spectrum of W 4f in Fig. 3c contains two peaks at the binding energy of 35.2 eV and 37.3 eV, illustrating that the main existing form of W is oxidized W ( $\text{W}^{6+}$ ) [31]. For the XPS spectrum of B 1s in Fig. 3d, it can be seen that the peaks are located at 188.1 eV and 192.0 eV which belong to elemental B and oxidized boron [32], respectively. In comparison with the bonding energy of 187.1 eV in pure B, the elemental B (188.1 eV) in  $\text{g-C}_3\text{N}_4/\text{Co-W-B/NF}$  catalyst produces a positive shift of 1.0 eV, signifying that the electron transfers from elemental B to vacant d-orbital of Co [33]. From the XPS spectrum of C 1s in Fig. 3e, it can be observed that there are three peaks located at 284.4, 285.5, and 288.8 eV, respectively. The first peak represents the C–C bond in carbon nitride. The other two peaks should belong to two different C in the heptazine ring in carbon nitride [34]. For the XPS spectrum of N 1s in Fig. 3f, it can be fitted three peaks centered at 398.7, 399.9, and 400.8 eV, which can be assigned to C = N – C, tertiary N atoms (N – (C)<sub>3</sub>), and amino-functionalized groups (C – N – H), respectively [35]. The above results indicate that Co–W–B and  $\text{g-C}_3\text{N}_4$  have been successfully loaded on the catalyst surface.

### Catalytic performance

Various  $\text{g-C}_3\text{N}_4/\text{Co-W-B/NF}$  samples prepared under different  $n_{\text{Co}^{2+}}:n_{\text{WO}_4^{2-}}$  values are applied to catalyze the hydrolysis of  $\text{NaBH}_4$  solution at 298 K. The test is carried out under darkness and visible light irradiation, respectively. The corresponding dehydrogenation curves are shown in Fig. 4a–d. It can be seen that the catalytic performance under visible light irradiation is better than that under darkness for the same  $\text{g-C}_3\text{N}_4/\text{Co-W-B/NF}$  sample. According to the linear fitting results, the HGR values of Co–W–B/NF and four  $\text{g-C}_3\text{N}_4/\text{Co-W-B/NF}$  catalysts are calculated. Figure 2S shows the kinetics curve of hydrogen generation of Co–W–B/NF. Figure 3S exhibits the comparison of HGR value for Co–W–B/NF catalyst in presence and absence of  $\text{g-C}_3\text{N}_4$ . The released  $\text{H}_2$  rate was calculated to be

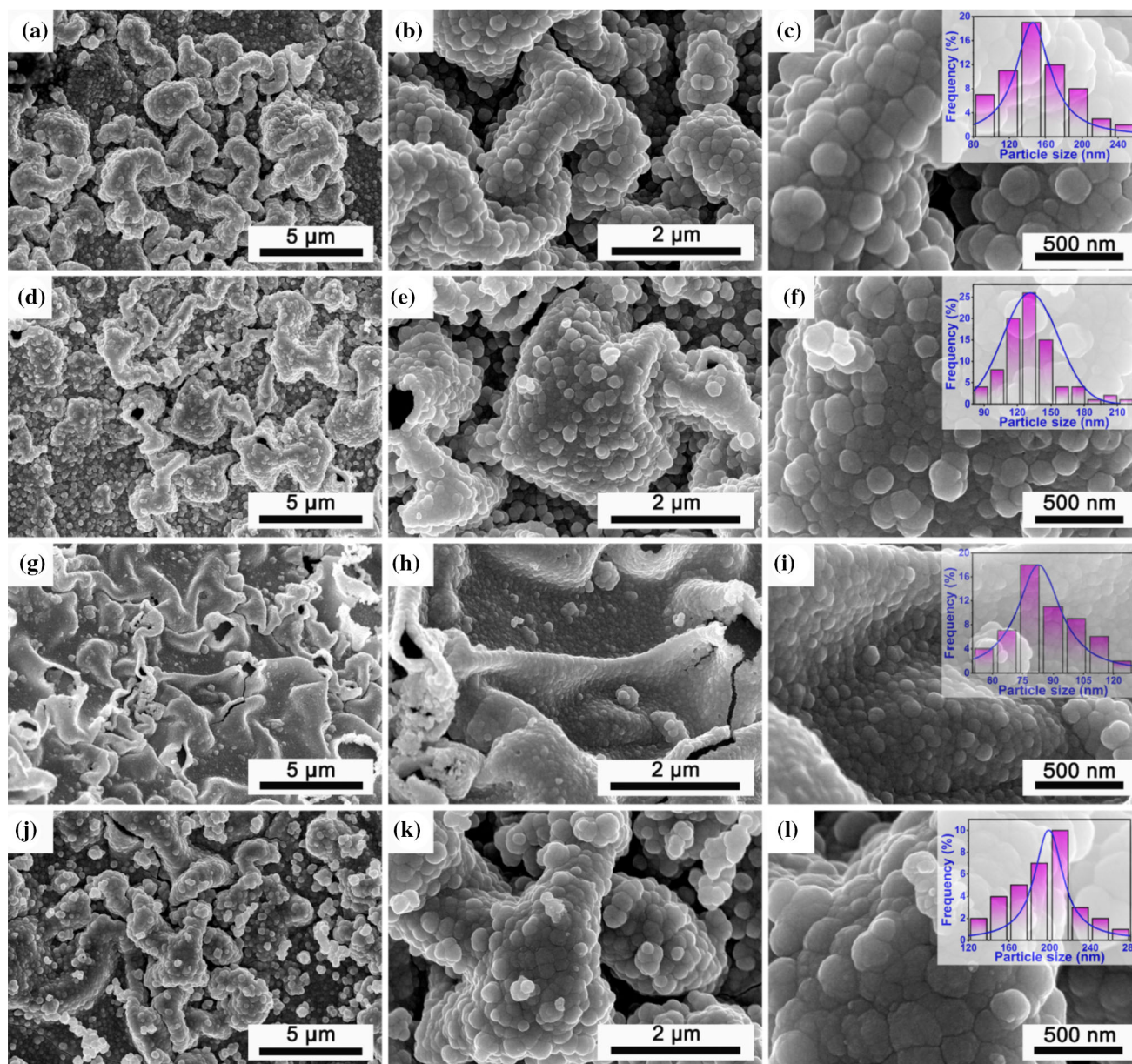


**Figure 2** SEM images and the corresponding size distributions of the  $g\text{-C}_3\text{N}_4/\text{Co-W-B/NF}$  samples prepared under different  $n_{\text{Co}^{2+}} : n_{\text{WO}_4^{2-}}$ : **a-c** 4:6, **d-f** 5:5, **g-i** 6:4 and **j-l** 10:0, respectively.

$5890 \text{ mL}\cdot\text{min}^{-1}\cdot\text{g}^{-1}$  for  $\text{Co-W-B/NF}$  catalyst in absence of  $g\text{-C}_3\text{N}_4$ , which illustrated that the HGR value was obviously lower than that of  $\text{Co-W-B/NF}$  in the presence of  $g\text{-C}_3\text{N}_4$ . Figures 4e and 5f display two comparison charts with the histogram and line chart, respectively. When  $n_{\text{Co}^{2+}} : n_{\text{WO}_4^{2-}}$  is 5:5, it can be found that  $g\text{-C}_3\text{N}_4/\text{Co-W-B/NF}$  exhibits a much better catalytic performance on the hydrolysis of  $\text{NaBH}_4$  under darkness and visible light irradiation. Especially under visible light irradiation, its HGR reaches  $7328 \text{ mL}\cdot\text{min}^{-1}\cdot\text{g}^{-1}$ , which has outperformed

$6191 \text{ mL}\cdot\text{min}^{-1}\cdot\text{g}^{-1}$  of single metal  $g\text{-C}_3\text{N}_4/\text{Co-B/NF}$  ( $n_{\text{Co}^{2+}} : n_{\text{WO}_4^{2-}} = 10 : 0$ ) catalyst. The best catalytic activity of  $g\text{-C}_3\text{N}_4/\text{Co-W-B/NF}$  ( $n_{\text{Co}^{2+}} : n_{\text{WO}_4^{2-}} = 5 : 5$ ) may be caused by the partial hollow structure, smaller particle size, loaded  $g\text{-C}_3\text{N}_4$ , and appropriate amount of added W.

### Effect of hydrolysis temperature

In order to study the influence of hydrolysis temperature on the  $\text{H}_2$  production of  $\text{NaBH}_4$  hydrolysis

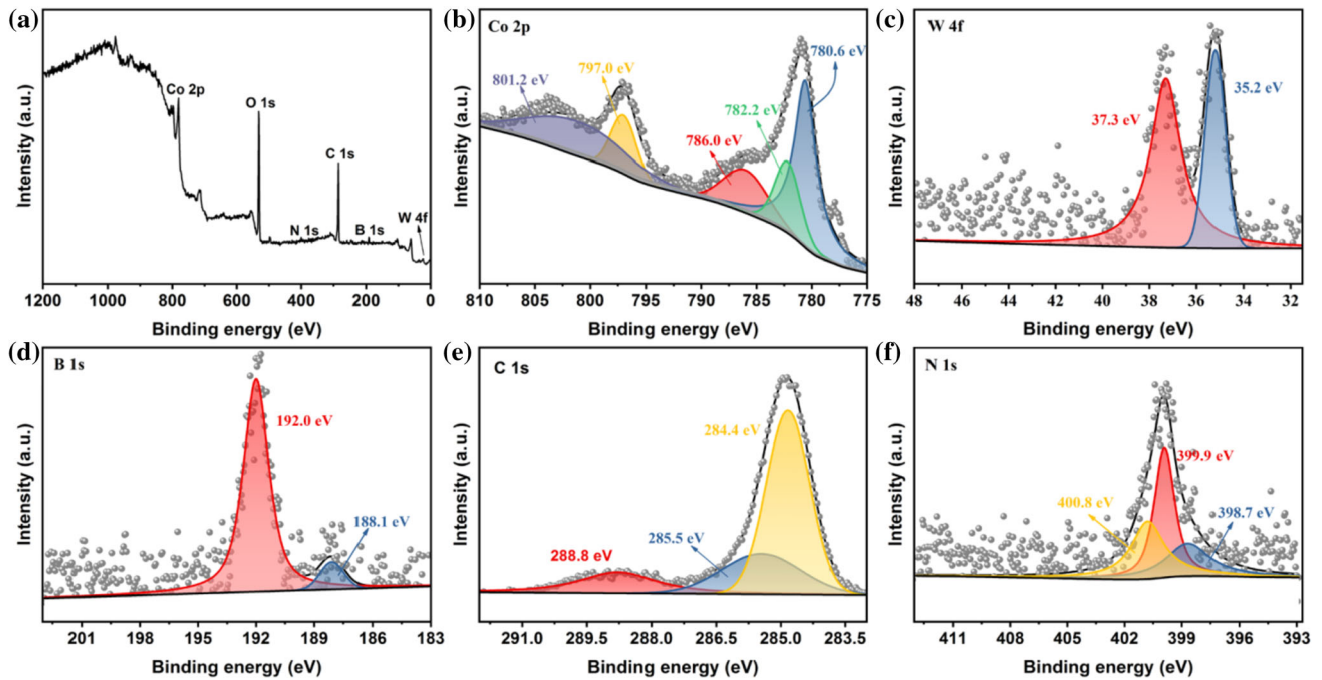


**Figure 3** XPS spectra of the as-prepared g-C<sub>3</sub>N<sub>4</sub>/Co–W–B/NF catalyst: **a** survey, **b** Co 2p, **c** W 4f, **d** B 1 s, **e** C 1 s and **f** N 1 s, respectively.

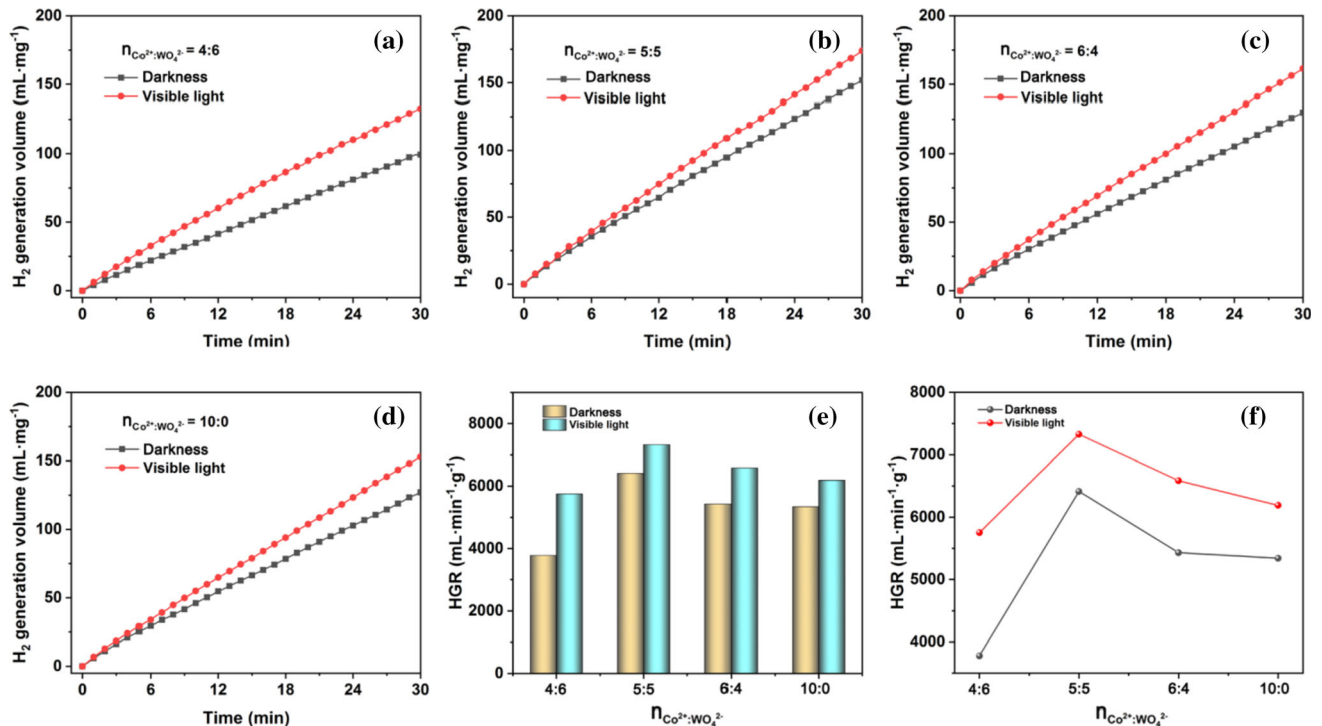


**Figure 4** **a–d** Plots of NaBH<sub>4</sub> hydrolytic H<sub>2</sub> production and **e, f** the specific HGR under darkness and visible light irradiation for the g-C<sub>3</sub>N<sub>4</sub>/Co–W–B/NF samples prepared under different n<sub>Co<sup>2+</sup></sub> : n<sub>WO<sub>4</sub><sup>2-</sup></sub> values: **a** 4:6, **b** 5:5, **c** 6:4, **d** 10:0, respectively.

by employing g-C<sub>3</sub>N<sub>4</sub>/Co–B/NF (n<sub>Co<sup>2+</sup></sub> : n<sub>WO<sub>4</sub><sup>2-</sup></sub> = 10 : 0) and g-C<sub>3</sub>N<sub>4</sub>/Co–W–B/NF (n<sub>Co<sup>2+</sup></sub> : n<sub>WO<sub>4</sub><sup>2-</sup></sub> = 5 : 5), the released H<sub>2</sub> tests are performed at different temperatures. As shown in

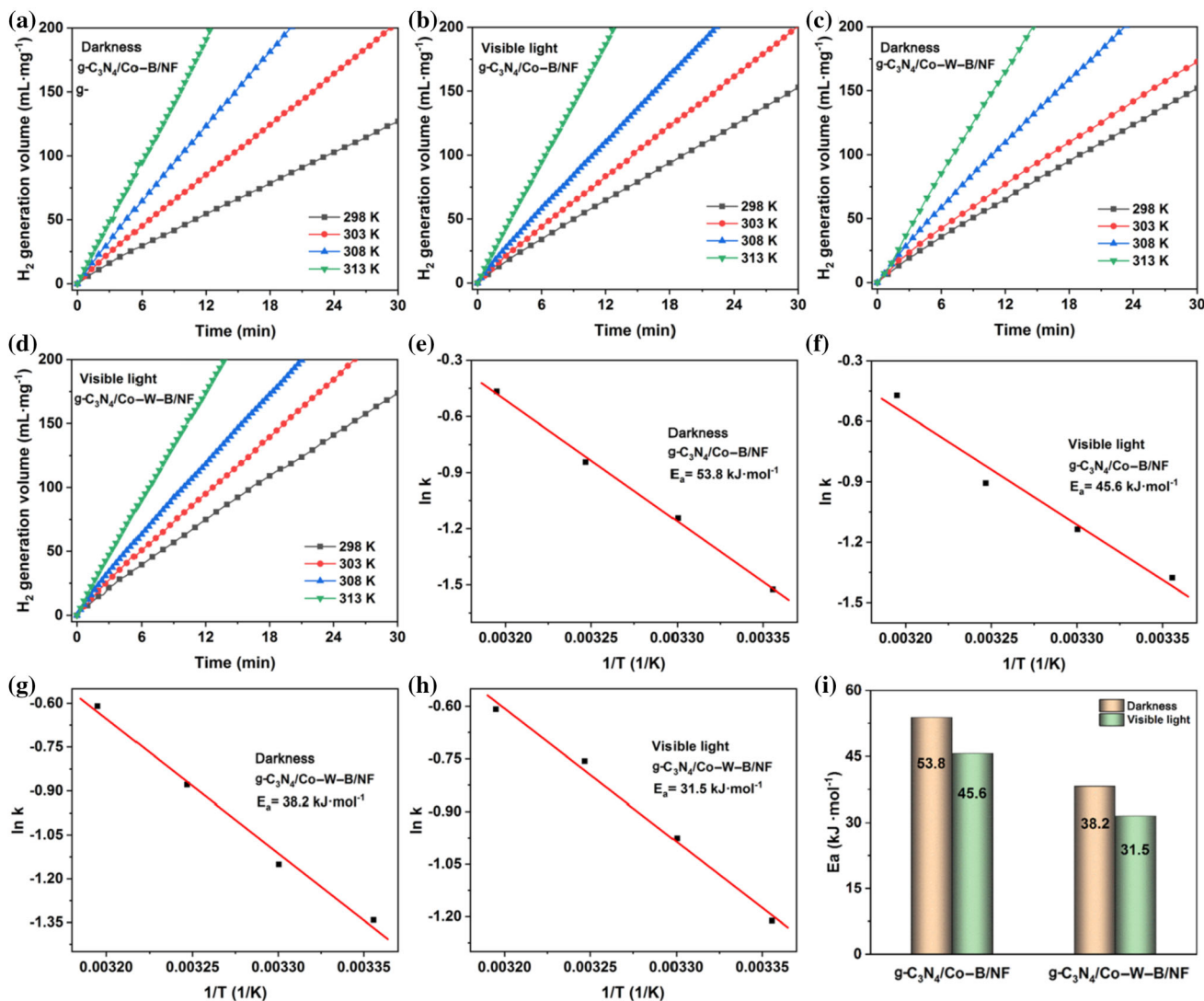


**Figure 5** Plots of NaBH<sub>4</sub> hydrolytic H<sub>2</sub> production at different temperatures and Arrhenius plot for g-C<sub>3</sub>N<sub>4</sub>/Co-B/NF **a, b, e, f** and g-C<sub>3</sub>N<sub>4</sub>/Co-W-B/NF **c, d, g, h** under darkness and visible light irradiation, respectively, **(i)** the corresponding E<sub>a</sub> comparison curve.

Fig. 5a–d, whether it is g-C<sub>3</sub>N<sub>4</sub>/Co-B/NF or g-C<sub>3</sub>N<sub>4</sub>/Co-W-B/NF, the hydrolysis H<sub>2</sub> generation rate under darkness and visible light irradiation significantly increases in the wake of the hydrolysis temperature increasing. Based on the relevant literatures [7, 36], it can be pointed out that the kinetic model for the catalyzed hydrolysis of NaBH<sub>4</sub> is zero-order reaction. The apparent activation energy (E<sub>a</sub>, kJ·mol<sup>-1</sup>) of g-C<sub>3</sub>N<sub>4</sub>/Co-B/NF and g-C<sub>3</sub>N<sub>4</sub>/Co-W-B/NF under darkness and visible light irradiation can be obtained through the following thermodynamic equation.

$$\ln k = \ln A - \frac{E_a}{RT} \quad (2)$$

In the above equation, *a* is the frequency factor, *R* is the general gas constant (8.314 J k<sup>-1</sup> mol<sup>-1</sup>), and *k* (mol min<sup>-1</sup> g<sup>-1</sup>) is the reaction rate constant, which can be calculated according to the linear part of the plot of NaBH<sub>4</sub> hydrolytic H<sub>2</sub> production at different temperatures. The Arrhenius plots (ln *k* versus 1/*T*) are presented in Fig. 5e–h. Under darkness, E<sub>a</sub> value is reckoned to be 53.8 kJ mol<sup>-1</sup> for g-C<sub>3</sub>N<sub>4</sub>/Co-B/NF and 38.2 kJ mol<sup>-1</sup> for g-C<sub>3</sub>N<sub>4</sub>/Co-W-B/NF, respectively. Under visible light irradiation, E<sub>a</sub> value is 46.5 kJ mol<sup>-1</sup> for g-C<sub>3</sub>N<sub>4</sub>/Co-B/NF and



31.5 kJ mol<sup>-1</sup> for g-C<sub>3</sub>N<sub>4</sub>/Co-W-B/NF, respectively. Figure 5i provides the Ea comparison curve between g-C<sub>3</sub>N<sub>4</sub>/Co-B/NF and g-C<sub>3</sub>N<sub>4</sub>/Co-W-B/NF under darkness and visible light irradiation. The results indicate that the Ea value under visible light irradiation is lower than that under darkness for the same catalyst. Under visible light irradiation, g-C<sub>3</sub>N<sub>4</sub>/Co-W-B/NF displays the lowest Ea value among the four situations. For the hydrolysis of NaBH<sub>4</sub> solution, the two parameters of HGR and Ea are important to evaluate the catalytic performance of the catalyst. Hence, the comparison of g-C<sub>3</sub>N<sub>4</sub>/Co-W-B/NF in this work with some catalysts reported for NaBH<sub>4</sub> hydrolysis is shown in Table 1 and Fig. 6. It should be pointed out that the reported data in Table 1 is gathered under normal condition and no visible light irradiation. Compared with the reported Co-W-B/Ni foam [37], it should be pointed out that the obtained g-C<sub>3</sub>N<sub>4</sub>/Co-W-B/NF catalyst in this work

was synthesized only by the electroless plating at room temperature. The active species for g-C<sub>3</sub>N<sub>4</sub>/Co-W-B/NF were different from reported Co-W-B/Ni foam according to the result of XRD (Fig. 1). In addition, g-C<sub>3</sub>N<sub>4</sub> was introduced in the catalyst system to investigate the photocatalytic characteristics for the hydrolysis of NaBH<sub>4</sub>. Therefore, they belonged to different catalyst systems and they had different composition. For the data in Table 1, the hydrolysis test was carried out under normal condition and no irradiation. From Fig. 6a, it can be seen that the HGR value of as-prepared g-C<sub>3</sub>N<sub>4</sub>/Co-W-B/NF is higher than of some reported Co-based catalysts [32, 38–52], Fe-Ni<sub>5</sub>P<sub>4</sub> [53], and Ru-IRA-400 [54]. As presented in Fig. 6b, except for Co-Ni-P-B [50], Co-W-B/Ni foam [37], Co-B-10CNTs [55], and Co-P-B [32], the obtained Ea is lower than that of most Co-B based [26, 38, 41–43, 46–49, 51, 52, 56, 57] and Co-P based [39, 40, 44, 45, 58] catalysts, Fe-Ni<sub>5</sub>P<sub>4</sub>

**Table 1** Comparison of HGR (a) and Ea (b) for NaBH<sub>4</sub> hydrolysis by employing g-C<sub>3</sub>N<sub>4</sub>/Co-W-B/NF ( $n_{\text{Co}^{2+}} : n_{\text{WO}_4^{2-}} = 5 : 5$ ) and some reported catalysts

Catalysts	Preparation method	HGR (mL·min <sup>-1</sup> ·g <sup>-1</sup> )	Ea (kJ·mol <sup>-1</sup> )	Refs.
Co-Ce-B/CSAC	Impregnation–reduction	16,420	48.2	[56]
Co-W-B/Ni foam	Electroless plating and calcination	15,000	29	[37]
Co-Ni-B/Cu sheet	Electroless plating	14,778.1	42.8	[57]
CoB/TiO <sub>2</sub>	Incipient-wetness impregnation	12,503	51.0	[26]
Co-B-10CNTs	Chemical reduction	12,000	23.5	[55]
Ru-SZ	Solegel method	9100	76	[59]
g-C <sub>3</sub> N <sub>4</sub> /Co-W-B/NF	Electroless deposition	7328	31.5	This work
Fe-CoP/Ti	Phosphidation reaction	6,060	39.6	[58]
Co-Mo-B	Co-deposition	4,200	43.7	[41]
Co-P-B	Chemical reduction	4,150	32	[32]
Co-Cu-B	Chemical reduction	3,554.2	52.0	[38]
Co-Cr-B	Chemical reduction	3,400	37	[47]
Co-B/attapulgitic clay	Impregnation and reduction	3,350	56.32	[46]
Mesoporous Co-B	Chemical reduction	3,350	40	[42]
Co-B hollow spheres	Template-assisted route	3,200	45.5	[48]
Co-Ni-B	Chemical reduction	2,608	62	[52]
Co-P/CNTs-Ni foam	Electroless plating	2,430	49.94	[40]
Co-Ni-P-B	Chemical reduction	2,400	29	[50]
Co-P/Cu sheet	Electroless deposition	1,846	48.1	[45]
Co-B/ Ni-foam	Chemical reduction	1,640	44.47	[49]
Co-Mn-B	Chemical co-precipitation	1,440	52.1	[43]
CoNiFeP	Electroless-deposition	1,128	54.26	[39]
Co-B/Carbon	Impregnation and reduction	1,127.7	57.8	[51]
Ru-IRA-400	Incipient wetness	606	56.0	[54]
Co-Ni-P/Pd-TiO <sub>2</sub>	Electroless deposition	460	57.0	[44]
Fe-Ni <sub>5</sub> P <sub>4</sub>	Hydrothermal reaction and phosphorization	175	53.41	[53]

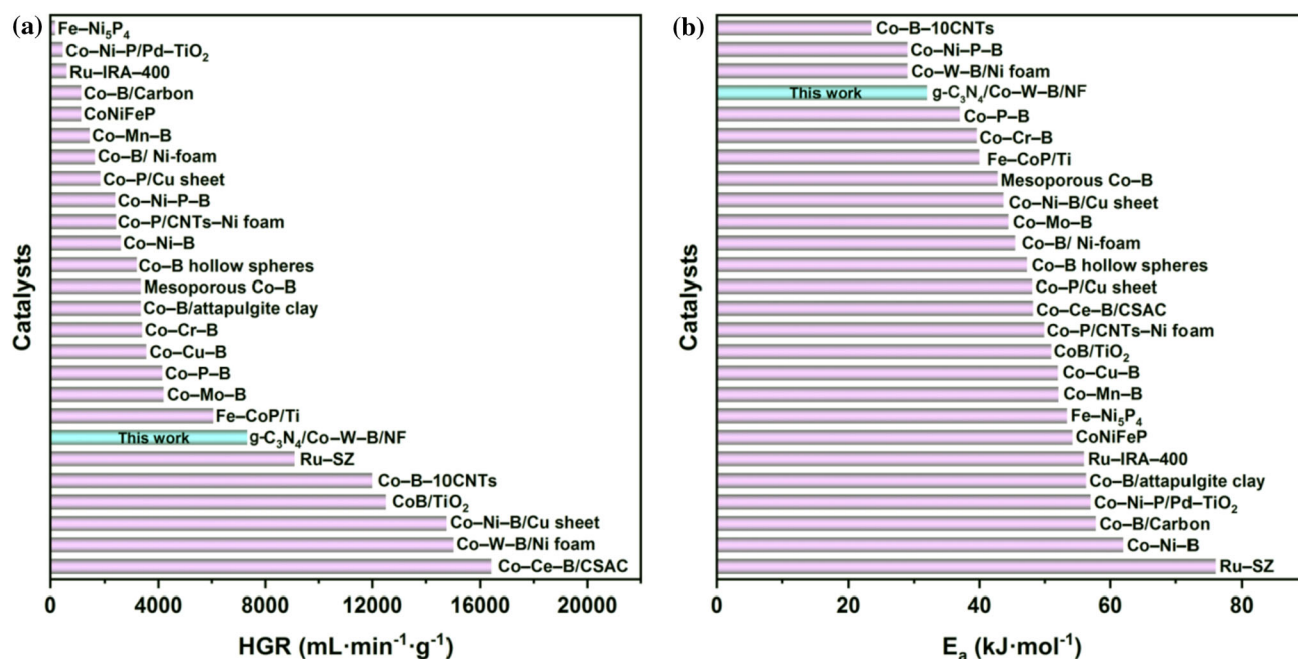


**Figure 6** Comparison curves of HGR (a) and  $E_a$  (b) for  $\text{NaBH}_4$  hydrolysis by employing  $\text{g-C}_3\text{N}_4/\text{Co-W-B/NF}$  ( $n_{\text{Co}^{2+}} : n_{\text{WO}_4^{2-}} = 5 : 5$ ) and some reported catalysts.

[53], Ru-SZ [59], and Ru-IRA-400 [54]. The above results indicate that the catalytic property of  $\text{g-C}_3\text{N}_4/\text{Co-W-B/NF}$  catalyst in this work is situated at the better rank.

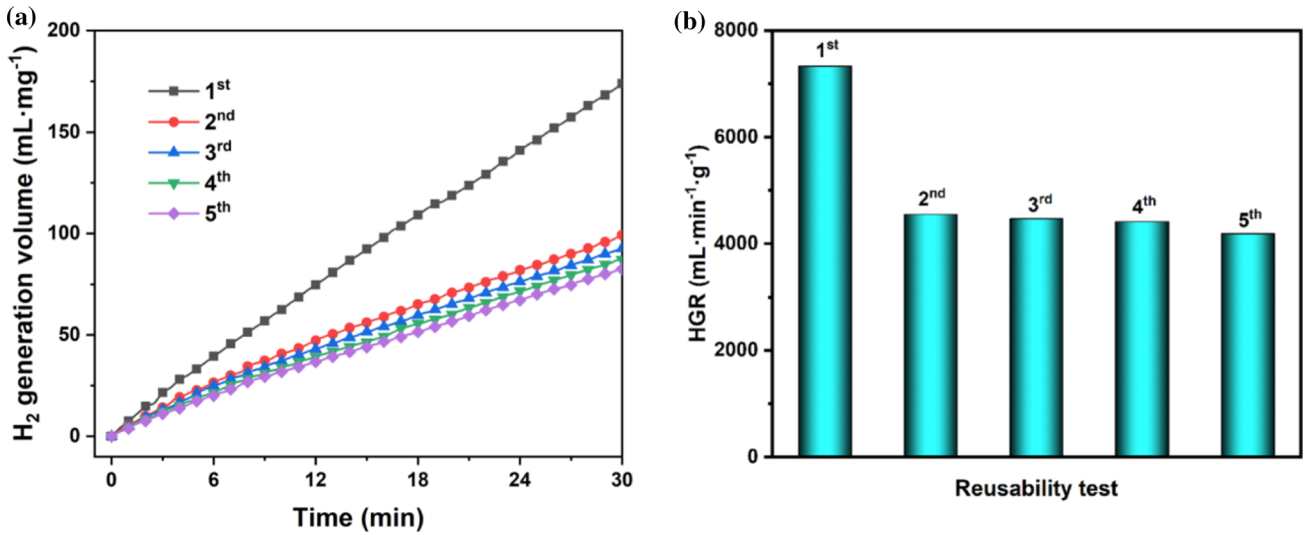
### Recycling ability

In order to investigate the reusability of the catalyst, the cyclic stability experiment of  $\text{g-C}_3\text{N}_4/\text{Co-W-B/NF}$  ( $n_{\text{Co}^{2+}} : n_{\text{WO}_4^{2-}} = 5 : 5$ ) toward the  $\text{NaBH}_4$  hydrolysis is carried out for five cycles under visible light irradiation at 298 K. The  $\text{H}_2$  production kinetics is revealed during multi-cycle experiments in Fig. 7a. Obviously, the slope in linear range is discrepant with the increase in cycle numbers. The corresponding specific HGR value is displayed in Fig. 7b. It can be seen that the HGR value is still maintained to  $4181 \text{ mL}\cdot\text{min}^{-1}\cdot\text{g}^{-1}$  after five cycles, which is still higher than that of ruthenium [60], Cu-Co [61],  $\text{CoNi@BN}$  [62], Ni/BN [63] used for the first time. Moreover, the HGR value of the as-obtained  $\text{g-C}_3\text{N}_4/\text{Co-W-B/NF}$  catalyst retains about 57% of its initial value. By analyzing the stability of other reported catalysts, it can be found that Co/Ni catalyst loses most of its catalytic activity just after 3 cycles [64], Co-W-P/Cu sheet catalyst retains about 51% of its initial activity [18], and Co/PCM catalyst maintains

about 68% of its initial activity after 2 cycles [65]. Hence, it can be inferred that the as-prepared  $\text{g-C}_3\text{N}_4/\text{Co-W-B/NF}$  catalyst is relatively stable in hydrolysis of  $\text{NaBH}_4$ .

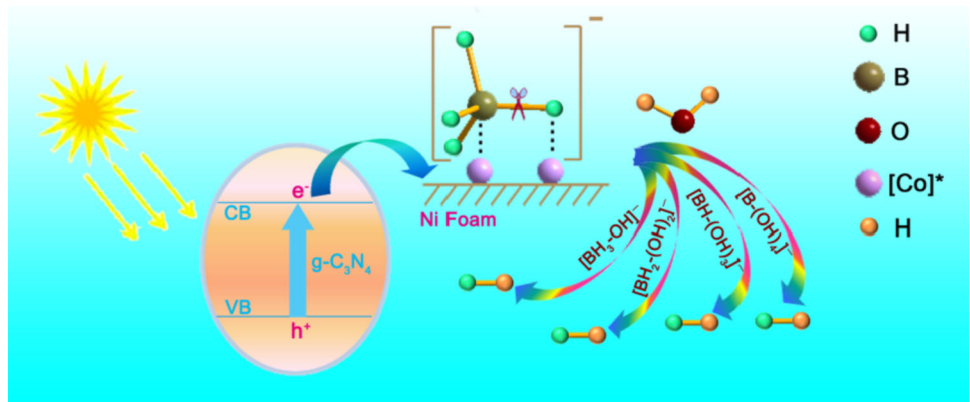
### Catalytic mechanism

Figure 7 shows a possible mechanism on  $\text{g-C}_3\text{N}_4/\text{Co-W-B/NF}$  ( $n_{\text{Co}^{2+}} : n_{\text{WO}_4^{2-}} = 5 : 5$ ) catalyst toward the  $\text{H}_2$  generation from the hydrolysis  $\text{NaBH}_4$  solution. Under visible light irradiation, the excited electrons generated from valence band (VB) to conduction band (CB) on  $\text{g-C}_3\text{N}_4$  might transfer to Co-W-B/NF, producing an electron-rich catalyst surface [23], increasing the quantity of hydrogen proton absorbed and reduce the bounding energy between the absorbed H and the catalyst, which would accelerate the  $\text{H}_2$  production and enhance the catalytic performance [66]. It may conducive to the enhancement of electrostatic interaction between the  $\text{NaBH}_4$  molecule and Co activated sites ( $[\text{Co}]^*$ ) on the surface of Co-W-B/NF catalytic system. In this case, borohydride ion ( $\text{BH}_4^-$ ) interacts with  $[\text{Co}]^*$  by electrostatic interactions. Then, the chemical bond of B-H cracks to form  $[\text{Co}]^*-\text{BH}_3^-$  and  $[\text{Co}]^*-\text{H}$ . After that, under the attack of  $\text{H}_2\text{O}$  molecule, the hydrolysis processes of

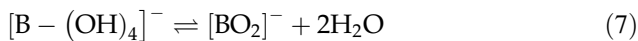
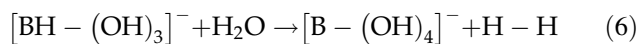
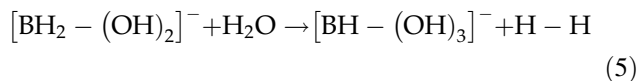
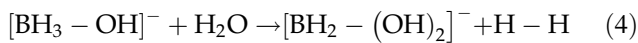
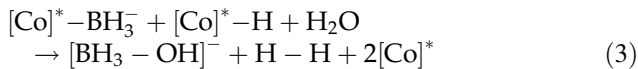


**Figure 7** a Recycling abilities of the as-prepared g-C<sub>3</sub>N<sub>4</sub>/Co-W-B/NF ( $n_{\text{Co}^{2+}} : n_{\text{WO}_4^{2-}} = 5 : 5$ ) in the hydrolysis of NaBH<sub>4</sub> under visible light irradiation at 298 K; b the corresponding histogram of HGR values during cycling process.

**Figure 8** Possible mechanism on g-C<sub>3</sub>N<sub>4</sub>/Co-W-B/NF ( $n_{\text{Co}^{2+}} : n_{\text{WO}_4^{2-}} = 5 : 5$ ) catalyst toward the H<sub>2</sub> generation from NaBH<sub>4</sub> hydrolysis.



H<sub>2</sub> generation are successively carried out as the following equations (Eqs. 3–7).



It needs to be noticed that the reactions of Eqs. 4–6 also take place on the surface of Co-W-B/NF. Different colors are employed to distinguish the H atom in NaBH<sub>4</sub> or H<sub>2</sub>O in Eqs. 3–7. Based on the aforementioned reaction processes, it can be concluded

that half of release H<sub>2</sub> toward the hydrolysis of NaBH<sub>4</sub> solution by applying g-C<sub>3</sub>N<sub>4</sub>/Co-W-B/NF comes from NaBH<sub>4</sub>, and the other half comes from H<sub>2</sub>O (Fig. 8).

### Conclusions

In summary, a simple synthetic strategy was applied to manufacture double-loaded g-C<sub>3</sub>N<sub>4</sub>/Co-W-B/NF catalysts. By changing  $n_{\text{Co}^{2+}} : n_{\text{WO}_4^{2-}}$  in the plating solution, different g-C<sub>3</sub>N<sub>4</sub>/Co-W-B/NF catalysts were obtained for catalyzing hydrolysis of NaBH<sub>4</sub> solution. When  $n_{\text{Co}^{2+}} : n_{\text{WO}_4^{2-}}$  value was 5:5, the as-prepared g-C<sub>3</sub>N<sub>4</sub>/Co-W-B/NF showed the best catalytic performance for NaBH<sub>4</sub> hydrolysis. Under visible light irradiation, the higher released H<sub>2</sub> rate of

7328 mL min<sup>-1</sup> g<sup>-1</sup> and lower activation energy of 31.5 kJ mol<sup>-1</sup> were achieved, which was superior to single metal g-C<sub>3</sub>N<sub>4</sub>/Co-B/NF catalyst, indicating that adding an appropriate amount of W played a significant role in promoting the catalytic performance in NaBH<sub>4</sub> hydrolysis. In addition, under visible light irradiation, the possible mechanism of the H<sub>2</sub> generation from NaBH<sub>4</sub> hydrolysis was proposed in the presence of g-C<sub>3</sub>N<sub>4</sub>/Co-W-B/NF catalyst.

## Acknowledgements

This work was supported by National Natural Science Foundation of China (22075186, 21975164), Key Laboratory of Advanced Energy Materials Chemistry (Ministry of Education) (111 project, B12015), the Natural Science Foundation of Liaoning Province (2022-MS-310), the Scientific Research Fund of Liaoning Provincial Education Department (LJKZ0993), the Revitalization Talents Program (XLYC1907013) of Liaoning Province, Liaoning Bai-QianWan Talents Program (2021921091), the Science and Technology Project of Shenyang (21-108-9-05, RC200393), the Hundred Talent Program (SSDBRJH1902002), and Major Incubation Project (ZD202003) of Shenyang Normal University.

## Declarations

**Conflict of interest** The authors declare that they have no conflict of interest.

**Supplementary Information:** The online version contains supplementary material available at <http://doi.org/10.1007/s10853-022-08073-z>.

## References

- [1] Fang X-J, Ren L-P, Li F, Jiang Z-X, Wang Z-G (2022) Modulating electronic structure of CoSe<sub>2</sub> by Ni doping for efficient electrocatalyst for hydrogen evolution reaction. *Rare Met* 41:901–910
- [2] Guang H-L, Zhu S-L, Liang Y-Q, Wu S-L, Li Z-Y, Luo S-Y, Cui Z-D, Inoue A (2021) Highly efficient nanoporous CoBP electrocatalyst for hydrogen evolution reaction. *Rare Met* 40:1031–1039
- [3] Huang J, Jiang Y, Li G, Xue C, Guo W (2017) Heterostructural NiTiO<sub>3</sub>/TiO<sub>2</sub> nanotubes for efficient photocatalytic hydrogen generation. *Renew Energy* 111:410–415
- [4] Zhang RL, Xie JW, Wang C, Liu J, Zheng XF, Li Y, Yang XY, Wang HE, Su BL (2017) Macroporous ZnO/ZnS/CdS composite spheres as efficient and stable photocatalysts for solar-driven hydrogen generation. *J Mater Sci* 52:11124–11134
- [5] Onat E, Çevik S, Şahin Ö, Horoz S, İzgi MS (2021) Investigation of high catalytic activity catalyst for high hydrogen production rate: Co-Ru@MOF. *J Aust Ceram Soc* 57:1389–1395
- [6] Wang T, Cao X, Jiao L (2021) Ni<sub>2</sub>P/NiMoP heterostructure as a bifunctional electrocatalyst for energy-saving hydrogen production. *eScience* 1:69–74
- [7] Schlesinger HI, Brown HC, Finholt AE, Gilbreath JR, Hoekstra HR, Hyde EK (1953) Sodium borohydride, Its hydrolysis and its use as a reducing agent and in the generation of hydrogen. *J Am Chem Soc* 75:215–219
- [8] Rossin A, Tuci G, Luconi L, Giambastiani G (2017) Metal-organic frameworks as heterogeneous catalysts in hydrogen production from lightweight inorganic hydrides. *ACS Catal* 7:5035–5045
- [9] Li L, Zhang Z-C, Wang Y-J, Jiao L-F, Yuan H-T (2017) Direct synthesis and dehydrogenation properties of NaAlH<sub>4</sub> catalyzed with ball-milled Ti-B. *Rare Met* 36:517–522
- [10] Brown HC, Brown CA (1962) New, highly active metal catalysts for the hydrolysis of borohydride. *J Am Chem Soc* 84:1493–1494
- [11] Wang C, Wang Q, Fu F, Astruc D (2020) Hydrogen generation upon nanocatalyzed hydrolysis of hydrogen-rich boron derivatives: Recent developments. *Acc Chem Res* 53:2483–2493
- [12] Kemmitt T, Gainsford GJ (2009) Regeneration of sodium borohydride from sodium metaborate, and isolation of intermediate compounds. *Int J Hydrogen Energy* 34:5726–5731
- [13] Zahmakiran M, Özkar S (2008) Intrazeolite Ruthenium(0) nanoclusters: a superb catalyst for the hydrogenation of benzene and the hydrolysis of sodium borohydride. *Langmuir* 24:7065–7067
- [14] Guo J, Wang B, Yang D, Wan Z, Yan P, Tian J, Isimjan TT, Yang X (2020) Rugae-like Ni<sub>2</sub>P-CoP nanoarrays as a bifunctional catalyst for hydrogen generation: NaBH<sub>4</sub> hydrolysis and water reduction. *Appl Catal B* 265:118584
- [15] Wang Y, Shen Y, Qi K, Cao Z, Zhang K, Wu S (2016) Nanostructured cobalt-phosphorous catalysts for hydrogen generation from hydrolysis of sodium borohydride solution. *Renew Energy* 89:285–294
- [16] Kim C, Lee SS, Li W, Fortner JD (2020) Towards optimizing cobalt based metal oxide nanocrystals for hydrogen generation via NaBH<sub>4</sub> hydrolysis. *Appl Catal A* 589:117303

- [17] Sahiner N, Ozay O, Aktas N, Inger E, He J (2011) The on demand generation of hydrogen from Co-Ni bimetallic nano catalyst prepared by dual use of hydrogel: As template and as reactor. *Int J Hydrogen Energy* 36:15250–15258
- [18] Guo Y, Dong Z, Cui Z, Zhang X, Ma J (2012) Promoting effect of W doped in electrodeposited Co-P catalysts for hydrogen generation from alkaline NaBH<sub>4</sub> solution. *Int J Hydrogen Energy* 37:1577–1583
- [19] Li XG, Bi WT, Zhang L, Tao S, Chu WS, Zhang Q, Luo Y, Wu CZ, Xie Y (2016) Single-atom Pt as Co-catalyst for enhanced photocatalytic H<sub>2</sub> Evolution. *Adv Mater* 28:2427–2431
- [20] Li X, Fan G, Zeng C (2014) Synthesis of ruthenium nanoparticles deposited on graphene-like transition metal carbide as an effective catalyst for the hydrolysis of sodium borohydride. *Int J Hydrogen Energy* 39:14927–14934
- [21] Guo LL, Gu XJ, Kang K, Wu YY, Cheng J, Liu PL, Wang TS, Su HQ (2015) Porous nitrogen-doped carbon-immobilized bimetallic nanoparticles as highly efficient catalysts for hydrogen generation from hydrolysis of ammonia borane. *Journal of Materials Chemistry A* 3:22807–22815
- [22] Liu M, Niu B, Guo H, Ying S, Chen Z (2021) Simple preparation of g-C<sub>3</sub>N<sub>4</sub>@Ni<sub>3</sub>C nanosheets and its application in supercapacitor electrode materials, hydrogen generation via NaBH<sub>4</sub> hydrolysis and reduction of p-nitrophenol. *Inorg Chem Commun* 130:108687
- [23] Navlani-García M, Verma P, Kuwahara Y, Kamegawa T, Mori K, Yamashita H (2018) Visible-light-enhanced catalytic activity of Ru nanoparticles over carbon modified g-C<sub>3</sub>N<sub>4</sub>. *J Photochem Photobiol, A* 358:327–333
- [24] Wang Y, Li G, Wu S, Wei Y, Meng W, Xie Y, Cui Y, Lian X, Chen Y, Zhang X (2017) Hydrogen generation from alkaline NaBH<sub>4</sub> solution using nanostructured Co-Ni-P catalysts. *Int J Hydrogen Energy* 42:16529–16537
- [25] Zhao J, Ma H, Chen J (2007) Improved hydrogen generation from alkaline solution using carbon-supported as catalysts. *Int J Hydrogen Energy* 32:4711–4716
- [26] Lu Y-C, Chen M-S, Chen Y-W (2012) Hydrogen generation by sodium borohydride hydrolysis on nanosized CoB catalysts supported on TiO<sub>2</sub>, Al<sub>2</sub>O<sub>3</sub> and CeO<sub>2</sub>. *Int J Hydrogen Energy* 37:4254–4258
- [27] Eom K, Cho K, Kwon H (2008) Effects of electroless deposition conditions on microstructures of cobalt-phosphorous catalysts and their hydrogen generation properties in alkaline sodium borohydride solution. *J Power Sources* 180:484–490
- [28] Karim AM, Su Y, Engelhard MH, King DL, Wang Y (2011) Catalytic roles of Co<sup>0</sup> and Co<sup>2+</sup> during steam reforming of ethanol on Co/MgO catalysts. *ACS Catal* 1:279–286
- [29] Narayanappa M, Dasireddy VDBC, Friedrich HB (2012) Catalytic oxidation of n-octane over cobalt substituted ceria (Ce<sub>0.90</sub>Co<sub>0.10</sub>O<sub>2-δ</sub>) catalysts. *Appl Catal A* 447–448:135–143
- [30] Genty E, Brunet J, Poupin C, Ojala S, Siffert S, Cousin R (2019) Influence of CO addition on the toluene total oxidation over Co based mixed oxide catalysts. *Appl Catal B* 247:163–172
- [31] Wang W, Yang S, Qiao Z, Liu P, Wu K, Yang Y (2015) Preparation of Ni-W-P-B amorphous catalyst for the hydrodeoxygenation of p-cresol. *Catal Commun* 60:50–54
- [32] Patel N, Fernandes R, Miotello A (2009) Hydrogen generation by hydrolysis of NaBH<sub>4</sub> with efficient Co-P-B catalyst: A kinetic study. *J Power Sources* 188:411–420
- [33] Li H, Li H, Dai W-L, Wang W, Fang Z, Deng J-F (1999) XPS studies on surface electronic characteristics of Ni-B and Ni-P amorphous alloy and its correlation to their catalytic properties. *Appl Surf Sci* 152:25–34
- [34] Xing W, Chen G, Li C, Sun J, Han Z, Zhou Y, Hu Y, Meng Q (2016) Construction of large-scale ultrathin graphitic carbon nitride nanosheets by a hydrogen-bond-assisted strategy for improved photocatalytic hydrogen production and ciprofloxacin degradation activity. *ChemCatChem* 8:2838–2845
- [35] Peng Y, Wang L, Liu Y, Chen H, Lei J, Zhang J (2017) Visible-light-driven photocatalytic H<sub>2</sub>O<sub>2</sub> production on g-C<sub>3</sub>N<sub>4</sub> loaded with CoP as a noble metal free cocatalyst. *Eur J Inorg Chem* 2017:4797–4802
- [36] Amendola SC, Sharp-Goldman SL, Janjua MS, Kelly MT, Petillo PJ, Binder M (2000) An ultrasafe hydrogen generator: aqueous, alkaline borohydride solutions and Ru catalyst. *J Power Sources* 85:186–189
- [37] Dai H, Liang Y, Wang P, Yao X, Rufford T, Lu M, Cheng H (2008) High-performance cobalt-tungsten-boron catalyst supported on Ni foam for hydrogen generation from alkaline sodium borohydride solution. *Int J Hydrogen Energy* 33:4405–4412
- [38] Wang Y, Zou K, Zhang D, Cao Z, Zhang K, Xie Y, Gong z, Li G, Bai S, (2020) Cobalt-copper-boron nanoparticles as catalysts for the efficient hydrolysis of alkaline sodium borohydride solution. *Int J Hydrogen Energy* 45:9845–9853
- [39] Kim DH, Jo S, Kwon J, Lee S, Eom K (2019) Effect of iron content on the hydrogen production kinetics of electroless-deposited CoNiFeP alloy catalysts from the hydrolysis of sodium borohydride, and a study of its feasibility in a new hydrolysis using magnesium and calcium borohydrides. *Int J Hydrogen Energy* 44:15228–15238
- [40] Wang FH, Zhang YJ, Wang YA, Luo YM, Chen YN, Zhu H (2018) Co-P nanoparticles supported on dandelion-like CNTs-Ni foam composite carrier as a novel catalyst for

- hydrogen generation from  $\text{NaBH}_4$  methanolysis. *Int J Hydrogen Energy* 43:8805–8814
- [41] Ke D, Tao Y, Li Y, Zhao X, Zhang L, Wang J, Han S (2015) Kinetics study on hydrolytic dehydrogenation of alkaline sodium borohydride catalyzed by Mo-modified Co–B nanoparticles. *Int J Hydrogen Energy* 40:7308–7317
- [42] Gupta S, Patel N, Fernandes R, Kothari DC, Miotello A (2013) Mesoporous Co–B nanocatalyst for efficient hydrogen production by hydrolysis of sodium borohydride. *Int J Hydrogen Energy* 38:14685–14692
- [43] Yuan X, Jia C, Ding X-L, Ma Z-F (2012) Effects of heat-treatment temperature on properties of Cobalt–Manganese–Boride as efficient catalyst toward hydrolysis of alkaline sodium borohydride solution. *Int J Hydrogen Energy* 37:995–1001
- [44] Rakap M, Kalu EE, Özkaz S (2011) Cobalt–nickel–phosphorus supported on Pd-activated  $\text{TiO}_2$  (Co–Ni–P/Pd– $\text{TiO}_2$ ) as cost-effective and reusable catalyst for hydrogen generation from hydrolysis of alkaline sodium borohydride solution. *J Alloys Compd* 509:7016–7021
- [45] Zhang X, Zhao J, Cheng F, Liang J, Tao Z, Chen J (2010) Electroless-deposited Co–P catalysts for hydrogen generation from alkaline  $\text{NaBH}_4$  solution. *Int J Hydrogen Energy* 35:8363–8369
- [46] Tian H, Guo Q, Xu D (2010) Hydrogen generation from catalytic hydrolysis of alkaline sodium borohydride solution using attapulgite Clay-supported Co–B catalyst. *J Power Sources* 195:2136–2142
- [47] Patel N, Fernandes R, Miotello A (2010) Promoting effect of transition metal-doped Co–B alloy catalysts for hydrogen production by hydrolysis of alkaline  $\text{NaBH}_4$  solution. *J Catal* 271:315–324
- [48] Ma H, Ji W, Zhao J, Liang J, Chen J (2009) Preparation, characterization and catalytic  $\text{NaBH}_4$  hydrolysis of Co–B hollow spheres. *J Alloys Compd* 474:584–589
- [49] Krishnan P, Advani SG, Prasad AK (2009) Thin-film CoB catalyst templates for the hydrolysis of  $\text{NaBH}_4$  solution for hydrogen generation. *Appl Catal B* 86:137–144
- [50] Fernandes R, Patel N, Miotello A (2009) Efficient catalytic properties of Co–Ni–P–B catalyst powders for hydrogen generation by hydrolysis of alkaline solution of  $\text{NaBH}_4$ . *Int J Hydrogen Energy* 34:2893–2900
- [51] Zhao J, Ma H, Chen J (2007) Improved hydrogen generation from alkaline  $\text{NaBH}_4$  solution using carbon-supported Co–B as catalysts. *Int J Hydrogen Energy* 32:4711–4716
- [52] Ingersoll JC, Mani N, Thenmozhiyal JC, Muthaiah A (2007) Catalytic hydrolysis of sodium borohydride by a novel nickel–cobalt–boride catalyst. *J Power Sources* 173:450–457
- [53] Ma T, Qiu Y, Zhang Y, Ji X, Hu P-A (2019) Iron-doped  $\text{Ni}_5\text{P}_4$  ultrathin nanoporous nanosheets for water splitting and on-demand hydrogen release via  $\text{NaBH}_4$  hydrolysis. *ACS Appl Nano Mater* 2:3091–3099
- [54] Amendola SC, Sharp-Goldman SL, Janjua MS, Spencer NC, Kelly MT, Petillo PJ, Binder M (2000) A safe, portable, hydrogen gas generator using aqueous borohydride solution and Ru catalyst. *Int J Hydrogen Energy* 25:969–975
- [55] Shi L, Chen Z, Jian Z, Guo F, Gao C (2019) Carbon nanotubes-promoted Co–B catalysts for rapid hydrogen generation via  $\text{NaBH}_4$  hydrolysis. *Int J Hydrogen Energy* 44:19868–19877
- [56] Zhang X, Li C, Qu J, Guo Q, Huang K (2019) Cotton stalk activated carbon-supported Co–Ce–B nanoparticles as efficient catalysts for hydrogen generation through hydrolysis of sodium borohydride. *Carbon Resources Conversion* 2:225–232
- [57] Wei Y, Meng W, Wang Y, Gao Y, Qi K, Zhang K (2017) Fast hydrogen generation from  $\text{NaBH}_4$  hydrolysis catalyzed by nanostructured Co–Ni–B catalysts. *Int J Hydrogen Energy* 42:6072–6079
- [58] Tang C, Zhang R, Lu W, He L, Jiang X, Asiri AM, Sun X (2017) Fe-doped CoP nanoarray: A Monolithic multifunctional catalyst for highly efficient hydrogen generation. *Adv Mater* 29:1602441
- [59] Demirci UB, Garin F (2008) Kinetics of Ru-promoted sulphated zirconia catalysed hydrogen generation by hydrolysis of sodium tetrahydroborate. *J Mol Catal A: Chem* 279:57–62
- [60] Basu S, Brockman A, Gagare P, Zheng Y, Ramachandran PV, Delgass WN, Gore JP (2009) Chemical kinetics of Ru-catalyzed ammonia borane hydrolysis. *J Power Sources* 188:238–243
- [61] Li C, Zhou J, Gao W, Zhao J, Liu J, Zhao Y, Wei M, Evans DG, Duan X (2013) Binary Cu–Co catalysts derived from hydrotalcites with excellent activity and recyclability towards  $\text{NH}_3\text{BH}_3$  dehydrogenation. *J Mater Chem A* 1:5370–5376
- [62] Fan D, Lv X, Feng J, Zhang S, Bai J, Lu R, Liu J (2017) Cobalt nickel nanoparticles encapsulated within hexagonal boron nitride as stable, catalytic dehydrogenation nanoreactor. *Int J Hydrogen Energy* 42:11312–11320
- [63] Yang XJ, Li LL, Sang WL, Zhao JL, Wang XX, Yu C, Zhang XH, Tang CC (2017) Boron nitride supported Ni nanoparticles as catalysts for hydrogen generation from hydrolysis of ammonia borane. *J Alloys Compd* 693:642–649
- [64] Akdim O, Demirci UB, Miele P (2011) Deactivation and reactivation of cobalt in hydrolysis of sodium borohydride. *Int J Hydrogen Energy* 36:13669–13675
- [65] Akdim O, Chamoun R, Demirci UB, Zaatari Y, Houry A, Miele P (2011) Anchored cobalt film as stable supported catalyst for hydrolysis of sodium borohydride for chemical hydrogen storage. *Int J Hydrogen Energy* 36:14527–14533

- [66] Guo J, Wu C, Zhang J, Yan P, Tian J, Shen X, Isimjan TT, Yang X (2019) Hierarchically structured rugae-like RuP<sub>3</sub>-CoP arrays as robust catalysts synergistically promoting hydrogen generation. *J Mater Chem A* 7:8865–8872

**Publisher's Note** Springer Nature remains neutral with regard to jurisdictional claims in published maps and institutional affiliations.

Springer Nature or its licensor (e.g. a society or other partner) holds exclusive rights to this article under a publishing agreement with the author(s) or other rightsholder(s); author self-archiving of the accepted manuscript version of this article is solely governed by the terms of such publishing agreement and applicable law.